PIRANHA: Project for InfraRed Astrometry aNd High Accuracy

Blue Team, Cabut, A., Dawson, P., Herrero-Illana, R., Meingast, S., Navarro-Gonzalez, J., Nizenkov, P., Saavedra, G., Schmid, D., Schreyer, K., Skjaeveland, A., Strandet, M., Sundl, M., Szalai, N., Vellutini, E., Warth, G., and Wende, H.

ABSTRACT

PIRANHA is a wide-field near-infrared astrometric space telescope designed to answer essential questions of modern astrophysics. The major goal is to measure the astrometric parallaxes of all galactic plane stars up to 1 kpc distant with an accuracy of 10%. Additional radial velocity measurements will establish a 3-D spatial motion map of both stars and substellar objects. This project will create the first full inventory of stars and substellar objects inside the visibly obscured plane of the Milky Way. PIRANHA can determine the Initial Mass Function (IMF) below 0.3 solar masses. In this respect previous astrometry missions and the planned Gaia mission are severely limited by extinction. For this reason they are unable to provide comprehensive data from typical star forming regions and young open clusters. PIRANHA can probe much deeper into cloudy environments and provide the data on very low mass stars and brown dwarfs that are needed to determine the IMF down to planetary level. Telescopes such as VLT, HST, JWST and Spitzer are not designed for these types of observations.

Key words. star formation – IMF – distance estimation – proper motion – radial velocity – galactic dynamics

1. Introduction

The shape of the IMF is well established and constrained for stars greater than $0.5\,M_\odot$. In comparison, determining the low mass part of the IMF, particularly in the substellar regime below $0.08\,M_\odot$ has proven more challenging. In this mass range the IMF may be affected by turbulent fragmentation, dynamical interactions, fragmentation of massive disks, photo-erosion of cores or other processes (see reviews by Whitworth et al. (2007) and Bonnell et al. (2007)). Hence in some theoretical scenarios there could be wide variations in the form of the IMF below about $0.3\,M_\odot$ depending on the environment. To test these competing theories it is necessary to collect enough data from sufficient numbers of different types of star forming regions to obtain results with insignificant errors. Ground based wide-field near-infrared surveys such as 2MASS and UKIDSS have greatly facilitated the search for low mass objects but have still not allowed the low-mass IMF to be sufficiently constrained. By combining recent observations using a combination of 2MASS and UKIDSS with results from Andersen et al. (2008), Dawson et al. (2011) indicate that the presence of OB stars is related to a higher abundancy of brown dwarfs, but note that this tantalising conclusion is only preliminary and needs to be substantiated by future surveys. As of today, low mass surveys in star forming regions suffer from two problems: (a) The surveys are incomplete, primarily due to strong and variable extinction in the molecular clouds. (b) It is difficult to isolate cluster members from background objects in the galactic plane that share similar photometry and proper motion.

Current analysis (Lodieu et al. (2006), Slesnick et al. (2006), Moraux et al. (2003), Bouvier et al. (2008)) relies firstly on colour-magnitude diagrams as shown in Figure 1. When allied with the well established models of Chabrier et al. (2000) this allows very accurate masses and ages to be assigned to individual members of star forming regions and young open clusters. Near-infrared colours are used as the spectral energy distributions of low mass stars and brown dwarfs peak in the range between 1 and 2.5 µm (Cushing et al., 2005). However photometric analysis alone cannot successfully identify cluster members. Other objects (e.g. distant AGB stars) may share similar photometry. Proper motion analysis can help to isolate cluster members but

this method is also fraught with problems. This is illustrated in Figure 2 which shows a typical vector point diagram. The motion of the cluster under investigation is obvious but the sample is clearly contaminated by objects with similar photometry that coincidentally share the same proper motion. This problem can be so bad in some regions e.g. Alpha Perseus (Barrado y Navascués et al., 2002) that the errors in the results do not allow for a robust testing of the IMF. Even in areas with very little contamination this method cannot provide the unbiased sample needed to test theories which predict that low mass stars/brown dwarfs and high mass stars will have different dispersion velocities.

2. Science case

2.1. Primary Science objectives

These problems can only be overcome by obtaining both spatial and dynamic information and near-infrared photometry for a much larger sample of objects than is currently available. Covering all nearby star forming regions and young open clusters (including all those in the Gould Belt) necessitates sampling 600 million near-infrared sources in or near the galactic plane. Distances of objects up to 1 kpc distant need to be measured to an accuracy of at least 100 pc. Radial velocities of objects have to be sampled to an accuracy of < 2 km/s.

As noted by Lindegren (2010) there are critical advantages to conducting such an astrometric mission in space. They include: (a) The absence of systematic and random errors caused by the atmosphere. (b) Weightlessness eliminates mechanical deformation of the instrument. (c) Space provides the more mechanically and thermally stable environment. (d) The entire sky is accessible from a single observatory. Radial velocities are an essential component of any astrometric study (Blaauw (1988), Perryman et al. (2001)) such as PIRANHA. While they could be measured from an observatory on Earth, Binney et al. (1997) emphasises that HIPPARCOS data was biased because of the lack of simultaneous acquisition of radial velocities. Cropper and Katz (2011) also describes the unsatisfactory situation caused by the lack of simultaneously acquired radial velocity in the HIPPARCOS survey. The necessity of simultaneously acquiring radial velocity data in a space based astrometry mission is further expounded
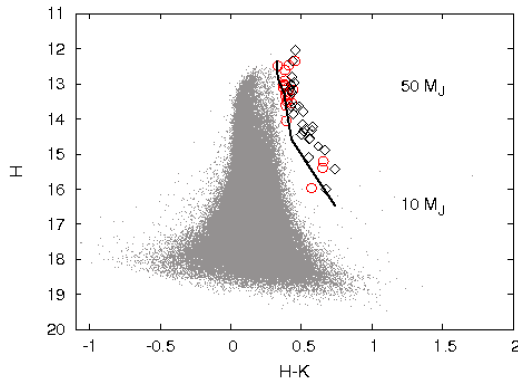
Fig. 1. A colour-magnitude diagram plotting H-K vs H for 300,000 objects in Upper Scorpius. The open diamonds and circles are objects of less than $0.09\,M_\odot$. The solid line is a Chabrier isochrone used to assign masses to the cluster members. Dawson, Scholz and Ray 2011 in press.
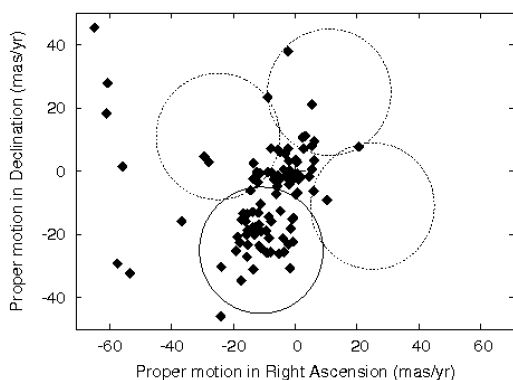
Fig. 2. Vector point diagram for photometric candidate members in Upper Scorpius. The cluster members are visible in the lower left solid circle. The contamination of the sample by non cluster members is clearly visible.

by Perryman et al. (2001) and Wilkinson et al. (2005) who notes that ground based surveys can always observe interesting objects with higher resolution spectroscopy after they have been revealed by the survey.

2.2. Legacy science

PIRANHA will produce a near-infrared source database of un-equalled scope and depth. This archive will provide extremely rich seams of extra data which can be mined by astrophysicists searching for answers on topics beyond star formation. Data provided by PIRANHA will be of great interest to those looking to solve the isolated star formation paradigm. Exploring the impact of binarity, which requires a clear separation of cooler and dimmer sources from hotter and brighter primaries, will be greatly facilitated. Persistent unanswered questions concerning the formation of the spiral arms and central bar of the galaxy will be made more amenable to solution. The field of galactic dynamics will benefit greatly from this new database of objects which have hitherto lacked information concerning all three components of their motion. PIRANHA data will also help constrain the age of stellar clusters by providing reliable dynamic information from its near-infrared measurements which can pinpoint the AGB turn-off. The identification and classification of stellar streams resulting from the merger of dwarf galaxies and globular clusters with the Milky Way will be greatly facilitated. It is also worth noting that PIRANHA data will complement the results of the Gaia mission by extending the range of wavelengths

observed from Gaia sources. It will also improve these results by providing extra data on objects which at Gaia's wavelengths are partially obscured.

3. Scientific requirements

The Primary Science Objectives will be achieved by assembling a catalogue of 600 million stellar and substellar objects. The distance of objects up to 1 kpc distant will be measured to an accuracy of 10%. With this data it will prove possible to provide cluster membership lists of objects down to a mass of $0.03\,M_\odot$ in nearby star forming regions. The astrophysical parameters of the objects of interest include (but are not limited to): intrinsic luminosity, mass, age, motion, distance, metallicity, cluster membership and temperature. The list of observable parameters it is necessary to obtain in order to correctly assign astrophysical parameters is comprised of: apparent luminosity, proper motion, radial velocity and spectral type. Therefore the science requirements contain several separate elements i.e. surveying, astrometric, photometric and spectroscopic requirements.

Surveying: Galactic plane sources have to be observed to a 100% completeness level at J = 19. A minimum two degree wide strip centred on the Galactic Plane will have to be covered to obtain sufficient sources. While the target is to cover all 360 longitudinal degrees of the Galactic Plane the survey shall cover a minimum of 270 degrees.

Astrometry: Positions on the celestial sphere will have to be measured to an accuracy of 0.1 mas.

Photometry: Observations shall be carried out in the Y, J, H and K infrared passbands which have effective wavelengths of 1.03, 1.25, 1.63 and 2.20 μm respectively. Photometric accuracy shall be at least 0.1 mag.

Spectroscopy: Spectra shall be measured in the range 2.29 to 2.39 μm with a spectral resolution of 20 000.

4. Instrumentation

Two instruments onboard PIRANHA will achieve the mission science goals: Large Infrared Camera Array (LICA) will obtain the astrometric measurements and photometry from the sources and Digital Micromirror Device Multi Object Spectrograph (DMDMOS) is a spectrograph used to determine accurate radial velocities of the targets. Both instruments are extensively explained in sections 4.2 and 4.3.

4.1. Optics

The telescope is a Cassegrain-RC design. Optical parameters are given in Table 1. A flat mirror behind the primary mirror reflects the focused light onto the detector plane, which is mounted on the wall of the detector housing. The secondary mirror is movable for focus calibration post-launch using the Gaia M2M position mechanism (Urgoiti et al., 2005).

4.2. Large Infrared Camera Array

Technical Description

The Large Infrared Camera Array (LICA) will allow precise measurements of astrometric positions of stars with an accuracy of 100 μas over a large range of magnitudes with simultaneously performed high precision photometry (see Figure 3). Therefore high spatial resolution and the ability to observe in four near-infrared (NIR) wavelength bands (Y, J, H, K) is required.

Table 1. Parameters of the telescope design

Total focal length:	74.26 m
Primary reflector (M1)	
Diameter:	3.50 m
Focal length:	2.65 m
Distance to M2:	2.50 m
Distance to focal plane:	1.50 m
Curvature:	-5.29 m
Secondary reflector (M2)	
Diameter:	0.20 m
Focal length:	-0.16 m
Distance to focal plane:	4.00 m
Curvature:	0.296 m

Fig. 3. Astrometric and photometric errors for different magnitudes. The astrometric error remains almost constant across a large dynamic range due to the adaptive observing strategy as described in the text. The photometric errors are eventually limited by confusion since this cannot be overcome by longer integration times. Here the errors are calculated for medium background (see text for details).

LICA utilizes a total of 64 Teledyne Hawaii-2RG Mercury Cadmium Telluride (HgCdTe) detectors assembled in 4 columns, corresponding to the requested four filters, with 2x8 detectors totaling in 67 million pixels per column. This large amount of pixels allows large sampling which is necessary to determine the astrometric positions precisely according to the science requirements.
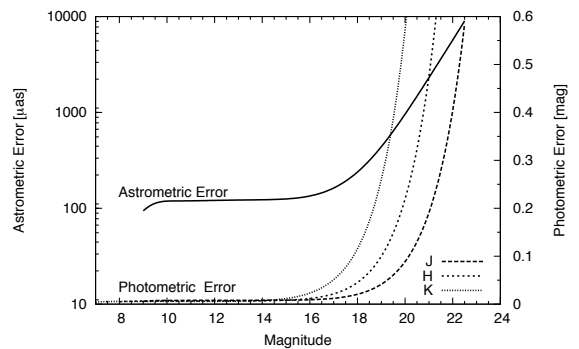
Each column is covered with one of the four NIR filters, therefore photometric magnitude measurements in the four bands can be obtained from the same image.

The Hawaii-2RG detectors are operated and read out by Teledyne SIDECAR ASICs (Application Specific Integrated Circuits) with a readout noise of $15\,e^-$. The Quantum Efficiency (QE) over a wavelength range from 1 to 2.5 μm is expected to be better than 85%. The SIDECAR ASICs (1 per detector) can perform a low-noise readout with 36 channels at 100 kHz in less than 2 seconds when using 12 bit dynamic range per channel. Comparable performance can be achieved with 16 bit conversions at the cost of a considerable increase in the data rate. Data of two detectors are collected by a Data Collection Unit (DCU) and transferred to each column's dedicated Data Processing Unit (DPU) which passes the processed data to the LICA Instrument Control Unit (ICU), which is connected via spacewire to the service module. DCUs, DPUs, the ICU, and one additional DPU reside in the Service Module (SVM) to reduce the complexity of the thermal control.

The additional DPU is dedicated to process selected data in order to estimate the movement of stars from the last filter onto the DMDMOS. This is required due to the observation strategy of the mission. Since the complete FOV is covered by four filters (equal in width), the spacecraft, after performing the observation of one FOV, will be shifted in steps of the filter width. This corresponds to a movements of 74 mm or 3.425 arcsec in the focal plane. The stars from the last filter column will move onto the DMDMOS where spectra are taken from individual sources being selected beforehand by the dedicated DPU. A critical requirement is an absolute pointing error of the satellite below 0.2 arcsec in order to guarantee that the positions of the sources on the DMD match the calculated mini-mirror locations.

Scientific Description

The key mission goals which can be achieved with LICA are very precise position determinations and photometric measurements in 4 filters. The position determination will be done by calculating the parallax of all stars detected in the survey. The position will be determined by calculating the centroid of the Point Spread Function (PSF), therefore sufficient sampling has to be taken into account. Zacharias and Dorland (2006a) state that for an astrometric step-stare mission a sampling of 2.5 is sufficient, but since the effective sampling also depends on wave-

length, a sampling of 4 in the K band was chosen. This also restricts the Field of View (FOV) for a given array size. In the case of the PIRANHA mission with 64 Hawaii-2RG detectors (including gaps) the FOV for LICA is then 220 arcmin². The error in position determination can be estimated with $\sigma = \frac{FWHM}{SNR}$, where SNR refers to the signal-to-noise ratio, which eventually determines the final error in the parallax measurement. The science requirements state that the error of a single position should be below 100 μas for a star at a distance of 1 kpc. An M0 star (which will represent a large sample of the provided database) at this distance with an extinction of $A_v = 10$ mag (taken from Nishiyama et al. (2009)) has an apparent magnitude of approximately $K = 16.4$ mag. This requirement was considered in the definition of the observing sequence. With the given setup and the predefined observing sequence this can be achieved with a SNR of 1 000. As a consequence small errors in the photometry can be achieved as well since $\sigma_m = 1.086 \cdot \frac{1}{SNR}$ (see Figure 3).

The understanding of the various noise components is therefore a critical science requirement. These components are: photon noise, dark current, readout noise, and background. In the following discussion the background contribution has been divided into diffuse background (e.g. originating from the Interstellar Medium, Zodiacal Light, etc.) and the confusion noise from faint undetected stars which is at its greatest towards the galactic plane. The SNR determinations were made by assuming blackbody radiation, but since this assumption is overoptimistic, the worst case for the different noise components was assumed. Since photon noise, readout noise, and dark current are not subject to change for a given source with a particular apparent magnitude and the PIRANHA instrumentation, the discussion here focuses on the background contributors.

An estimation for the diffuse background emission has been taken from a model based on COBE observations (Kelsall et al., 1998). The worst case for diffuse emission corresponds to $0.1\frac{MJy}{sr}$ which translates to 0.12 Jy in the total FOV. The estimations about the second background component, the confusion noise, are based on extrapolated point source counts in the galactic GLIMPSE survey (Benjamin et al., 2005), the 2MASS All Sky Data Release documentation on data processing (Section IV.5.g), and 10 σ detections. Based on this, the confusion noise has been estimated at 4 Jy distributed over the whole FOV. The amount of photons collected from confusion noise is therefore large, but one also has to take into account that all of them are distributed over the whole image (268 Mpix).

The contribution to the confusion noise by asteroids in the solar system was estimated using the *Infrared extension of the Statistical Asteroid Model model* (IRSAM) (Kiss et al., 2008)
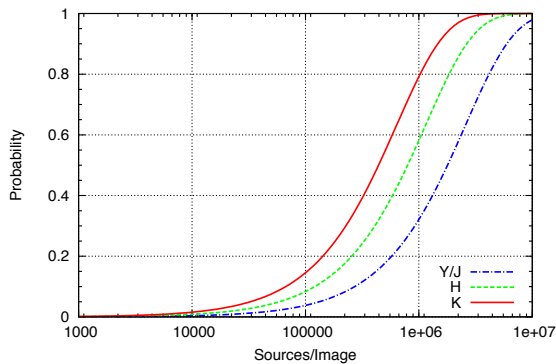
Fig. 4. The probability of finding a second source within a limited range around a detected source. For surveys the probability should be kept below 0.3 which translates into a range of 10^5 to 10^6 sources in the total FOV.

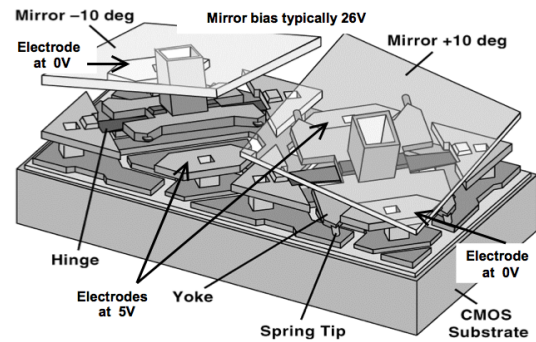**Fig. 5.** Sketch of two DMDs. A. B. Sontheimer (2002).

and was found to be negligible in NIR compared to unresolved background source counts, which is reasonable since most of the emission occurs in longer wavelength regimes ($\geq 10\,\mu m$) (see lecture Kiss, Alpbach 2011). As source counts increase dramatically towards the galactic center the densest regions in the galaxy cannot be mapped due to confusion.

An important parameter for the confusion is the probability of finding a second source within a limited range around a detected source. The probability depends upon the resolution of the telescope and the source density. For surveys the probability should be in the range of 0.1 to 0.3 (see lecture Kiss, Alpbach 2011) which corresponds to a range of 10^5 to 10^6 sources in one image (see Figure 4). This range will certainly be exceeded towards the galactic center (estimations based on GLIMPSE), therefore significant degradation in data quality towards the densest regions is expected.

Based on these estimations an imaging observing sequence with adaptive detector integration time (DIT) has been generated to encompass both a large dynamic range (DR) and high SNR as required by the astrometry. The observing sequence consists of 7 different integration times, ranging from $0.02\,s$ to $60\,s$, each done 2 times on 3 dithered positions.

A possible alternative to the adaptive DIT method would be to use very short fixed integration times (e.g. 0.01 s) to make sure that the brightest stars do not saturate and to stack many exposures (NDITs). Such an approach was rejected because the sensitivity would decrease by two orders of magnitude as the noise contribution from background and readout overcome the actual signal from the source.

The total exposure time per field was correlated with the spectroscopic integration time, optimized to allow an overhead for on-board calculations and still maintain high DR. Furthermore, a dither pattern was integrated to allow bad-pixel rejection, cover the gaps between the single chips and increase the DR even further. The stabilization of the satellite after a dither movement has been preliminary estimated to be about $60\,s$ and was taken into account to make sure that the errors in the centroid calculation are not dominated by inaccurate pointings. To finally arrive at an estimation for the SNR and therefore photometric and astrometric errors, the different noise components have been merged. Figure 3 shows these errors as a function of apparent magnitude in different filters. For fainter magnitudes where no DIT adjustment takes place ($K > 16$), the background noise takes over very fast. The confusion limit for medium crowded fields (as calculated with the estimations above) e.g. in K is 20.5 mag. This highly depends on the pointing direction of the satellite, since source counts dramatically increase towards the galactic center.

On the other hand the confusion limit will decrease to fainter magnitudes for less crowded fields.

Since the zero-point in the flux measurements will change during the mission lifetime (radiation damage, etc.) a calibration has to take place in regular intervals. These adjustments can be based on ground based absolute flux calibrations.

### 4.3. Digital Micromirror Device Multi-Object Spectrograph

The science objectives dictate that radial velocities (RVs) obtained by the Digital Micromirror Device Multi-Object Spectrograph (DMDMOS) have to be measured in a wavelength range that allows us to see deep into dark clouds, hence K-band spectroscopy is the logical choice.

Spectral range

The spectral window observed should be as small as possible in order to be compatible with telemetry restrictions. At the same time it should contain a sufficient number of lines to allow measurements of RVs accurately. We have decided to use the window spanning 2.29 - 2.39 μm, where it is possible to find six CO transitions ($^{12}CO(2-0)$, $^{12}CO(3-1)$, $^{13}CO(2-0)$, $^{12}CO(4-2)$, $^{13}CO(3-1)$ and $^{12}CO(5-3)$) that are easily identified in G-, K- and M-type stars and substellar objects. The end of the Pfund series from hydrogen, which is present in A- and F- stars, is also within that range and complementing this is a weak but detectable Na doublet already found in F- and G-type stars (see Wallace and Hinkle (1997) and Liermann et al. (2009)).

Digital Micromirror Device

In the FOV there will be several stars, so multi object spectroscopy is needed. There are three ways of creating a multiple object spectrograph (MOS). Either micro-shutters, fiber based MOS or a Digital Micromirror Device (DMD) are used. DMDMOS uses DMDs because micro-shutters have experienced a lot of problems on NIRSPEC and the disadvantage with fibres is that only a few hundred can be used, and a lot more is needed for this mission. Another problem with fibers is that there is a larger loss of throughput than in DMDs. In Rochester Institute of Technology (RIT) the DMD is being used for the first time in combination with spectroscopy in the instrument RITMOS. DMDMOS is using the technology used in RITMOS to develope a spectrograph optimised for multi object observations of RVs in the NIR. A Texas Instruments DMD is used for this. In Figure 5 the basic principle of DMD is shown. Flipping the mirrors occurs when one electrode is on high (5 V), and the other on low (0 V), and a mirror bias of 26 V is applied. For more information on RITMOS and DMDs see Meyer et al. (2004). The DMD is composed of 800x3200 mirrors (Zamkotsian et al.,
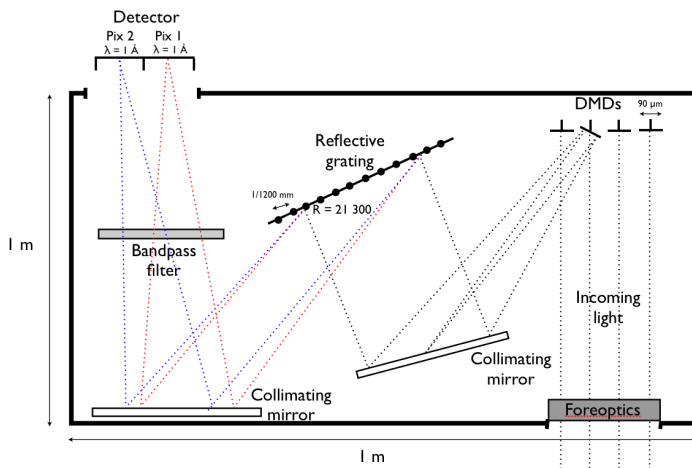
Fig. 6. The basic design of the spectrograph. Not to scale. The light falls on the DMDs, whereafter it is reflected onto a collimator mirror, a reflecting grating, another collimator mirror, through a band-pass filter and onto the detector.

2011) each with a length of 90 μm. The size of the mirrors chosen based on the PSF occupies 4×4 pixels (to be conservative 5×5 is used), each with a length of 18 μm. These mirrors replace the slit masks in conventional grating spectrographs and give the opportunity of observing 4000 spectra individually in one observation. A MOS is already in use at the SUBARU telescope, and a NIR MOS (IRMOS) using DMDs is currently under development, see Kearney and Ninkov (1998).

Optical path

Prior to spectrometric observation, the positions of the stars selected are calculated in an onboard micro controller, based on the photometric observations of the same FOV. The available calculation time depends on the exposure time of the spectrograph, and is much smaller than this. From these calculations the micromirrors individually deflect the incident light from the selected objects into the spectroscopy path. This is done by tilting the DMDs 10° in less than 1 μs.

Hereafter the deflected light passes through a collimator where it is parallelised before it hits a reflecting grating. It then passes through a collimator, a band-pass filter to restrict the dispersion to one order, and finally onto the detector. The basic spectrograph design is shown in Figure 6.

DMD data processing

To select objects for spectroscopy, the micro-controller will need to reduce the data to a certain degree. First the dark frame and the flatfield frame must be subtracted to obtain the highest possible SNR for the next calculations. After this the positions of maximum flux must be found, and on the basis of this, the objects will be selected. If an object should fall onto more than one mirror, all these mirrors will turn to ensure we get the object. If however several objects fall on the same horizontal line the system needs to make sure that all objects are observed. The micro controller must do this in less than 3 minutes.

Schematic of the data processing and instrumental control was discussed in section 4.2.

Spectrograph

Our science requirements are not far from what the RITMOS instrument delivers, but it will be necessary to change the design
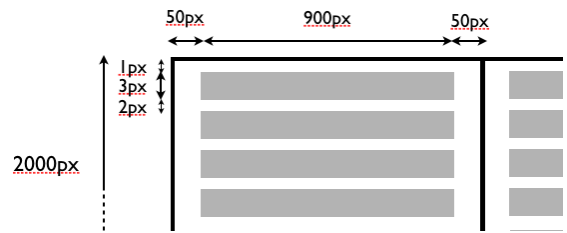
Fig. 7. Diagram of a section of the detectors that shows how the pixels are used to avoid the spectra overlapping.

a bit for PIRANHA. The details and optimisation of the design should be done by an expert in the field. The RITMOS fits into a box of approximately 0.5m×0.3m×0.3m. Room has been made for a box of 1m x 1m x 1m on the spacecraft to be sure that we can fit in the spectrograph with any necessary design changes. The mass of the spectrograph is estimated to be 100 kg based on the masses of the individual elements.

The detector is of the same sort as that used for the photometry. In DMDMOS 4 detector modules are used sitting in a 2×2 configuration, with 2000×2000 pixels in each. The spectrum from one object is dedicated 1000×5 pixels, 900 for the spectra with 50 pixels on each side to avoid overlapping of spectra (see Figure 7). In addition each spectra is projected onto 3 rows to avoid pixel errors, and one row on each side is used to avoid overlapping of spectra in this direction. The detectors are split into two columns each, to ensure that the spectrum of each star is projected into a separate row of pixels. In total it is possible to get 3 200 spectra in one observation.

A reflecting grating is chosen to obtain a high resolution and linear dispersion. The dedicated space for DMDMOS is 900 pixels per spectrum and since our spectral range is 0.1 μm the wavelength resolution is 1.1Å/pixel and thereby a resolution power of ~21 400 is obtained. We assume (in a similar way to Gaia) that by fitting the lines to Gaussians, we can get a resolution 10 times better, that is ~0.1 Å/pixel, yielding a velocity resolution of 1.28 km/s. Assuming a 15th magnitude star in the K-band, and a SNR of 5 we need an exposure time of 11 min. With a lower limit magnitude of 15 mag, it will be possible to observe small (20 M_{Jup}) Brown Dwarfs out to a distance of 150 pc (Lodieu et al., 2006).

If a low magnitude star is lying within the PSF of a larger star, it could become impossible to detect. As seen in Figure 4, this is the case for 1%, 10%, 30% of the stars in the K-band if there is 10 000, 100 000 or 300 000 stars respectively in the FOV. This could be solved by using a DMD to project the emission from larger star away from the detectors. The problem however is that a DMD will introduce uncertainties in the astrometry measurements, which will lower the precision of positions. This problem does not arise for spectroscopy, as the same accuracy is not needed.

For calibration an in-situ Th-Ar lamp is used, because it allows calibration immediately after observation. The lines could e.g. be Th I λ 2378.83Å, λ 2371.12Å and λ 2367.93Å. For more lines see Kerber et al. (2008).

Disadvantages of DMDs

DMDs are not without disadvantages: although there are some evaluations for space applications, such low temperatures might cause trouble in the mirror actuators. The lifetime of the DMDs under normal operating conditions exceeds 100 000 hours. Although the spectrograph only need to operate for 44 000 hours the very low temperature might change the effective lifetime. Another issue to consider is the gap between the mirrors, that can cause light to reflect off the metal substrate

Table 2. Specification for DMDMOS

Spectroscopy	
Purpose	measurements of multi object high resolution radial velocities
Central wavelength	2.34 µm
Delivered wavelength range	2.29 - 2.39 µm
Resolution Power	1.1 Å @ 23400 Å $\rightarrow R = \frac{\lambda}{\Delta\lambda} \approx 21300$
Dispersion	55 Å/mm (1.1 Å/pixel for a detector with 18 µm pixels)
Calibration	A Th-Ar lamp is used
Design parameters specific to DMDMOS	
Field of view	0.062 ° × 0.250 °
Instrument size	1m × 1m × 1m
Mass	∼ 100 kg
Power supply	20 W

Fig. 8. Measurements taken for every star.

where the mirrors are assembled and cause scattering. The array of micro-mirrors have a strong diffraction pattern that has to be taken into account as well. Finally, if there are several stars aligned, in the x-direction it will only be possible to get spectra of a maximum of four of them simultaneously due to our design constraints.

5. Data

5.1. Data processing

The in-situ data processing is described in section 4.3. The data processing on-board will first reduce the amount of data by a factor of 2, and it will hereafter be compressed by yet another factor of 2 before it is transmitted to the ground station.

PIRANHA will obtain an enormous amount of data which will need processing. The data reduction process will vary from that of Gaia due to the different mapping procedure. The concept of a stare mission is described in Zacharias and Dorland (2006b). In case of PIRANHA the observed sky fields in each band overlap each other by 25%. The first step of the image correction is subtraction of bias-frames, dark-frames and flat-field frames. Hereafter a PSF fitting procedure that finds the x,y pixel coordinates of the individual objects must be developed. From positions along the entire 360° survey, an astrometric consistent solution has to be found using known positions of quasars and other visible very distant point-like objects from the Gaia catalogues. These will work as a master grid. A concern could be lacking quasar observation so near the galactic plane, but some counterparts of quasars has been found at very low galactic latitude.

5.2. Data calibration, release and archiving

We suggest that the Science Archives Team (SAT) at ESAC operate and maintain the archive. Half a year after launch a science verification will be released and every half year there will be a data release until the mission is finished, whereafter the final version of the data will be released. The data will be archived and available for the users.

6. Observation strategy

The objectives of the mission are to cover ±1° of the Milky Way around the galactic plane three times each six months (or each n.5 years). We need to measure parallax. Three pictures of the same star are required in order to deduce parallax and a correction due to its proper motion. Considering an orbit at the Lagrange point L2 of the Sun/Earth system, this mission will require at least 6
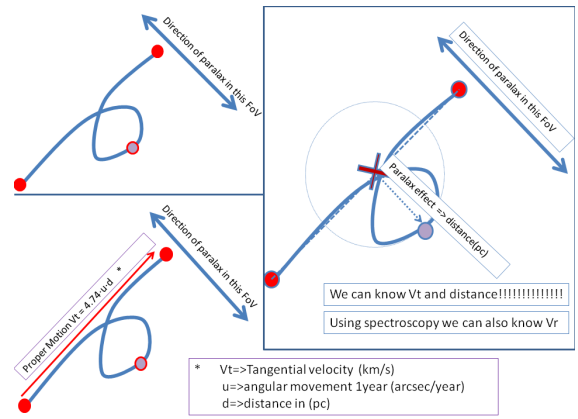
years. In one day of observation, as our simulations show, we have only 1° per day for latitude scanning with respecto to the ecliptic frame. The first year and a half will be dedicated to the scanning of a range of 1° of one half of the Milky Way, three times, centered on the galactic plane. In order to do that, the satellite is rotated 180° after the first 6 months and again after the first year. After 1.5 years, the first results will be available while the satellite continues to scan the other half of the Milky Way. In three years 1° of the Milky Way will be covered three times. The next three years will be dedicated to the scanning of the rest of the Milky Way (0.5° above 1.5° of the galactic plane and 0.5° below -1.5° of the galactic plane). That way, new results will be available each 1.5 year. Each day the satellite moves in narrow columns of 1° of ecliptic latitude, scanning as many columns as possible with a maximum of 1° longitude scanned per day to maintain an acceptable orientation with the Sun.

7. Parallax/proper motion measurements

Due to the orbit of the satellite around the Sun, stars will have a periodic proper motion. In order to measure the distance of one star, we also need its proper motion. This can be achieved by taking two pictures of this star at the same position on the orbit to avoid the parallax effect. Then we need a third picture of the same star in the opposite direction with respect to the orbit to have the maximum parallax effect. Due to the fact that PIRANHA measures stars only close to the galactic plane oriented close to 90° to the L2-Earth Orbit, we have a well defined direction of parallax effect in each FoV and we can reduce mathematical free parameters needed to calculate the proper motion and the distance of the stars (Miklós, 1998).

8. Mission requirements

Table 3. A summary of the mission requirements

Mission Requirements	
Mission lifetime	6 years
Survey area	2 x 360 along the galactic plane
Target orbit	L2 Halo
Absolute Pointing Error	< 0.1 arcsec
Relative Pointing Error	< 50 marcsec
Data amount	800 Gbits/Day
Operating Temperature Optics	100 K

9. Orbit

The L2 orbit was chosen for several reasons: it provides a thermally stable environment while performing survey at a constant solar angle. The demanding pointing requirements benefit by having only the solar radiation pressure as a disturbance. The transfer and the orbit are considered to be eclipse-free by proper selection of the launch window.

10. Launcher

The Ariane 5 ECA launcher was chosen due to the mass, dimensions of the spacecraft and the orbit required. The fairing dimensions and launcher adapter were considered in the design of the spacecraft in order to define the spacecraft configuration. The transfer duration to the L2 orbit is one month and the spacecraft only requires a $\Delta V \simeq 76$ m/s to perform a perigee velocity variation and transfer correction maneuvers after a direct insertion into L2 provided by the launcher.

11. Spacecraft

The spacecraft design is based on Wertz (2008).

11.1. Attitude and Orbit Control System

The requirements of the Attitude and Orbit Control System (AOCS) are driven by an APE of 0.1 arcsec and a RPE of approximately less than 50 mas. Moreover, the spacecraft will have to perform a *stop-and-stare* strategy in order to be able to obtain the frames required during the survey. These two requirements demand fine pointing combined with good agility in order to perform the survey in the required mission lifetime. The coarse pointing performed during non-science phases of the mission, will be achieved with the help of a star tracker and gyroscopes for the attitude determination. For fine pointing a Fine Guidance System (FGS), which is part of the focal plane, is used. The FGS will allow attitude estimates with known error in the order of 10 mas which is required to meet the pointing requirements. Conventional star trackers would only provide error information in the order of 1 arcsec. Safe mode will be implemented with the help of sun sensors and gyroscopes. The actuator selection is also driven by the pointing requirements. Two options were considered: Gaia cold gas system and magnetic bearing reaction wheels. Conventional wheels were dismissed since their micro vibrations would only allow an RPE in the order of 200 mas to be reached. In a trade-off between a cold-gas thruster system and reaction wheels, the mass of both systems were calculated. The decision for the Magnetic Bearing Reaction Wheels (Rockwell Collins) was supported by propellant mass over 1 ton for the cold-gas system. Also their static and dynamic imbalance is at least one order of magnitude better than conventional wheels. The wheels allow precise actuation and stabilization while granting low mass properties with respect to the cold-gas system. Also they will allow the stop and stare maneuvers to be performed more efficiently in terms of time resources. The actuator used during safe mode and orbital correction maneuvers is based on monopropellant propulsion system.

11.2. Structure

A top-level schematic of the spacecraft can be seen in Figure 9. The structure of the spacecraft was divided into four basic elements: the sunshield, service module (SVM), payload module (PM) and baffle. Optical system and bench are made of Silicon Carbide (SiC). The sunshield is made of carbon fiber reinforced

Table 4. The Mission Overview

AOCS	
Requirements	Absolute Pointing Error: < 0.2 arcsec
	Relative Pointing Error: < 50.0 marcsec
Sensors	Star Tracker
	Sun Sensors
	Gyroscopes
	Fine Guidance System (FGS)
Actuatora	Thrusters (Monopropellant hydrazine)
	Magnetic Bearing Momentum Wheels
STRUCTURE	
	Honeycomb covered with layers
Material	Aluminum
	Carbon Fiber Reinforced Polymer
	Multi-Layer Insulation
TCS	
Method	Passive Cooling
Operating Temperatures	Optics and Payload Module at 100K
	Service Module at 300K
Radiators	Maximum Power Dissipation: 15.3W
COMMUNICATION	
Specifications	K-Band
	100GB/Day
Spacecraft	High-gain antenna (0.4m diameter)
	Low-gain antenna (X-band)
	Transponder
Ground station	35 m diameter antenna
	Possible downlink duration: 8.5h
DATA	
Equipment	Leon3 Processor
	NAND Flash memory
POWER	
Solar array	Required power generation: ca. 1272W
	Gallium Arsenide (Efficiency 28%)
	Degradation for 5 years: 0.87
	Total Area: 6.3 m^2
Li-ion battery	2 hours of autonomy
	DOD: 0.6
	Discharge efficiency: 0.9
PCDU	Regulated to 28V
	Up to 1500W

polymer (CFRP) and on the front side solar arrays are mounted. The available area for solar array is significantly greater than the required one for the spacecraft; therefore there is a lot of growth capacity in case of increased power consumptions demands. The reverse side is covered with multi-layer insulation (MLI) to guarantee low radiation towards the baffle and the optical system inside. The service module, which contains all the avionics equipment as well as the instrument warm electronics, is made of aluminum honeycomb. The payload module and the integrated optical bench (including the bipods holding the optical bench) are made of Silicon Carbide (like the primary mirror) in order to guarantee an athermal design of the telescope, that would reduce the thermo-elastic effects in order to improve optical quality performance. The baffle material is CFRP. For the mass approximation the SVM assumed an equally distributed hexagon with stiffening structures in each corner. The launcher adapter interface selected is 2624 and it allows a central cone to connect the launcher interface up to the optical bench interface (diameter of 3.5 m) with SVM providing higher stiffness than adapters of fewer diameters.
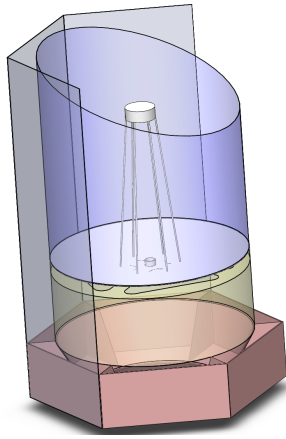
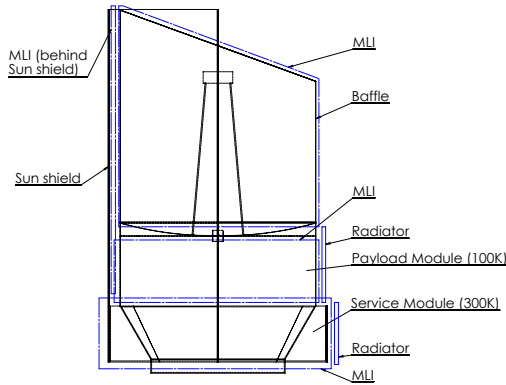**Fig. 9.** A top-level schematic of the spacecraft.

Fig. 10. Thermal concept of spacecraft.

11.3. Thermal Control System

Figure 10 shows the thermal concept of the spacecraft, which is passive to reduce system complexity. For a preliminary estimate it was divided into 4 elements. As mentioned before the reverse side of the sun shield is covered with MLI-insulation. Moreover, the SVM, PM and baffle are covered with MLI. For the SVM a working temperature of 300 K is assumed in order to guarantee the thermal environment required for the avionics. PM including the optics is operated at an operating temperature of 100 K. The selection of the primary mirror in Silicon Carbide (SiC) allows operation it at 100 K with excellent thermal expansion (CTE) performance. At the same time, it is possible to couple the instrument and telescope operating temperature to mitigate possible IR thermal load from telescope to detectors. The area on the cold side of the spacecraft allows the use of radiators up to a size that can dissipate around 15 W of power, which is more than sufficient to dissipate the power generated by the read-out electronics. It should be considered that the service module and optical bench might need heating, but the sunshield offers enough area for additional solar arrays. Furthermore, the option of removing the sun shield by introducing a baffle with several layers could be exploited in the future to improve the mass resources as well as the spacecraft configuration concept.

11.4. Telecommunications

The large amount of data generated by the two instruments requires the use of K-band for the science data downlink. Around 800 GBits/day are downloaded with a rate of 65 Mbps. A 0.4 m-diameter high-gain antenna is required and using either Cebreros or Malargue ESA ground stations. This is achieved with 4 hours visibility per day at sufficient elevation. This visibility per day is achievable by a seasonable combination of two ground stations. Housekeeping telemetry and telecommand performed via 2 low-gain antennas (LGA) uses X-band.

11.5. Data handling

For the on-board data handling a Leon3 processor is used. The temporary data storage is achieved with NAND flash memory. The storage capacity is sized for 3 days. The communication with spacecraft units is performed via $MIL-STD-1553$ bus and with the mass memory unit as well as instruments via Spacewire.

11.6. Power Budget

The total power required is estimated to be around 1.2 kW for the nominal mode and 560 W for the safe mode. The power generation is performed with solar cells mounted on the front side of the sun shield. The battery is sized to account for 2 hours after launcher release and initial sun acquisition phase since the orbit is eclipse-free. The batteries selected are Li-ion (130 Wh/kg). The PCDU and harness were taken into account as part of the EPS design.

Table 5. Power budget

Power budget	Operation Mode [W]	Safe Mode [W]
Payload	574.6	-
AOCS	250.8	228.0
Communication	174.0	178.0
OBC	61.0	61.0
Power	76.3	76.3
Total	1136.7	539.3
Margin	20%	20%
Total with margin	1364.0	647.2

11.7. Mass budget

Mass approximations were made for all forementioned subsystems. A margin of 20% for each subsystem and a system margin of 20% were applied to the dry mass. Based on the dry mass with system margin the propellant mass was calculated. Moreover, the harness was considered with 10% of the dry mass.

Table 6. Mass budget

System	Mass (kg)	Mass(%)
AOCS	159.5	5.4
Electrical Power System	70.5	2.4
Communications and Data	14.4	0.5
Thermal Control System	113.5	3.8
Propulsion	56.8	1.9
Payload	533.4	18
Structure	1467.4	49.4
On Board Computer	43.2	1.5
Propellant	214.7	7.2
Harness	295	9.9
Total	2968.5	100
Margin of 20 %	593.7	
Total with margin	3562.2	

Table 7. Cost analysis for PIRANHA

	M€	%
Structure	105.0	9.1
Thermal control	40.9	3.5
Propulsion	17.0	1.5
Mechanism	9.9	0.9
Harness	10.6	0.9
Solar array	22.1	1.9
Batteries	5.7	0.5
Power conditioning	3.2	0.3
Data handling	62.1	5.4
AOCS	96.4	8.3
Reaction wheel	47.5	4.1
Telecommunications	17.3	1.5
Telescope	320.2	27.6
DMDMOS	92.4	8.0
LICA	28.2	2.4
Payload electronics	31.2	2.7
Ground segment and operations	100.0	8.6
Ariane 5 launcher	150.0	12.9
Total	1159.8	100

12. Operating modes

Launch Mode: During the launch only fundamental avionics are kept on (after the powered phase of the Ariane5 launcher). Then others subsystems will be started for the transfer to L2 orbit after separation.

Transfer Mode: The attitude control is ensured by reaction wheels. Solar panels provide the energy. Instruments are off. Orbital corrections maneuvers ae performed with thrusters.

Observation Mode: The observation mode is separated into two phases. In the first phase, the coarse pointing of star is ensured by the star tracker and the gyros and the motion is provide by the reaction wheel. The star tracker allows the accuracy (APE) of 1". The final accurate is obtained via the fine guidance sensors and reaction wheels adjusted the pointing to an accuracy of 0.01".

Safe Mode A safe mode has also been defined, in this mode, gyros and thrusters maintain the pointing orientation. The science instruments are shut down but the telecommunication is maintained.

13. Cost analysis

The cost analysis was carried out considering the mass and the technical complexity of each component. The payload costs are mainly driven by DMD for DMDMOS and heritage detector level (JWST and HST). Six years of operation in $L2$ orbit were considered with respect to ground segment and mission operations costs. Table 7 shows the expected costs for PIRANHA mission.

14. Time schedule

In Figure 11 you can see the schedule of PIRANHA. Time delay may occur in the phases B2/C/D due to critical technical requirements, such as the DMDss, the number of Hawaii-2RG detectors and the manufacturing, polishing and testing of the 3.5 m SiC primary mirror.
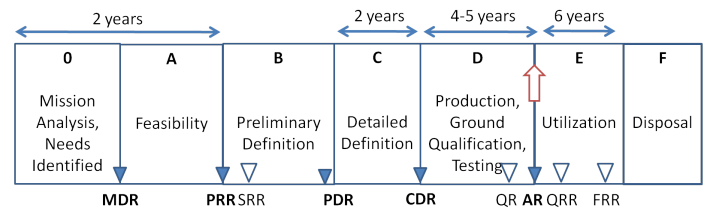
Fig. 11. Time schedule for PIRANHA.

15. Critical points

Table 8. Mission risk assesment. Critical system, consequences, risk and severity are shown. A-E likelihood of occurrence, from minimum (A) to maximum (E). 1-5 severity of occurence, from minimum effect (1) to critical (5).

Risk assessment			
Critical system	Consequence	Risk	Sev.
Attitude/orbit control system (AOCS)			
Fine guidance sensor (FGS) on focal plane, payload module becomes part of AOCS	Design and testing of avionics more complex	B	2
Magnetic bearing wheels (MBW) not yet qualified (TRL < 5)	Pointing accuracy critical for spectrometry, photometry can manage with less accurate pointing	C	5
Communications			
K-band downlink: ESA Deep Space Network not yet upgraded to K-band	Cannot fly before comm link is ready.	B	1
Optics			
Primary mirror: 3.5m mirror critical technology	2m mirror gives 1/3 sensitivity: mission viable but takes longer.	D	4
Detector			
Digital Multimicromirror Device (DMD) not yet fully space-qualified	Critical for spectroscopy. Operating DMD at 200 K would greatly complicate thermal control.	C	5
Hawaii-2RG detector: Need nominally 68 detectors + test detectors. ITAR-restricted, production capacity low	Critical technology, cannot fly without. Can use a reduced sensor using fewer detectors, at the cost of FOV and mission time.	C	4
Computer			
Large data volume produced, must be processed and reduced onboard before downlink	Manageable (cmp. f.ex. Gaia mission)	B	2

16. Descoping options

There are a two options for descoping the mission. The first is to reduce the primary mirror to one with a diameter of 2 m. This gives an effective area of 3.13 m^2, and decrease the angular resolution from 0.2 to 0.32 arcsec. The consequence of a smaller effective area is an increase in integration time for the photometry by a factor of 3 and the integration time for the spectroscopy

rises. This means that the telescope must be kept stable for a longer time, which can become a challenge. As we cannot expect the mission to last for 3×6 years, the area covered on the sky must be reduced. The second option for descoping is to use less detectors. The consequence of this is a smaller FOV, which again will reduce the survey area. It is clear that both possibilities will reduce the amount of science gained from this mission.

17. Conclusion

We have designed a space telescope which will answer essential questions of modern astrophysics. The design arrived at is capable of achieving the requirements that the primary science objectives demand. The performance of the telescope is expected to exceed all minimum performance goals. A significant database legacy will be generated. This can be mined for new insights by succeeding generations of scientists. It will yield answers to questions that go beyond the field of star formation. It will significantly enhance and extend the results of the Gaia mission. PIRANHA's design builds on the heritage of previous missions. Proven technology is used whenever practical and cutting edge technology wherever necessary. Engineering PIRANHA will significantly push the envelope of industrial and research capability. It will leave a rich heritage for use in future missions.

PIRANHA will add immeasurably to the store of human knowledge. It will define our grasp of the Initial Mass Function for years to come. It will explore Milky Way dynamics and spiral arm structure. It will observe what no other mission has observed before.

References

Andersen, M., Meyer, M. R., Greissl, J., and Aversa, A. (2008). Evidence for a Turnover in the Initial Mass Function of Low-Mass Stars and Substellar Objects: Analysis from an Ensemble of Young Clusters. *ApJ*, 683:L183–L186.

Barrado y Navascués, D., Bouvier, J., Stauffer, J. R., Lodieu, N., and McCaughrean, M. J. (2002). A substellar mass function for Alpha Persei. *A&A*, 395:813–821.

Benjamin, R. A., Churchwell, E., Babler, B. L., Indebetouw, R., Meade, M. R., Whitney, B. A., Watson, C., Wolfire, M. G., Wolff, M. J., Ignace, R., Bania, T. M., Bracker, S., Clemens, D. P., Chomiuk, L., Cohen, M., Dickey, J. M., Jackson, J. M., Kobulnicky, H. A., Mercer, E. P., Mathis, J. S., Stolovy, S. R., and Uzpen, B. (2005). First GLIMPSE Results on the Stellar Structure of the Galaxy. *ApJ*, 630:L149–L152.

Binney, J. J., Dehnen, W., Houk, N., Murray, C. A., and Penston, M. J. (1997). The Kinematics of Main Sequence Stars from HIPPARCOS Data. In R. M. Bonnet, E. Høg, P. L. Bernacca, L. Emiliani, A. Blaauw, C. Turon, J. Kovalevsky, L. Lindegren, H. Hassan, M. Bouffard, B. Strim, D. Heger, M. A. C. Perryman, & L. Woltjer, editor, *Hipparcos - Venice '97*, volume 402 of *ESA Special Publication*, pages 473–478.

Blaauw, A. (1988). ESO's early history, 1953 - 1975. I. Striving towards the convention. *The Messenger*, 54:1–9.

Bonnell, I. A., Larson, R. B., and Zinnecker, H. (2007). The Origin of the Initial Mass Function. *Protostars and Planets V*, pages 149–164.

Bouvier, J., Kendall, T., Meeus, G., Testi, L., Moraux, E., Stauffer, J. R., James, D., Cuillandre, J.-C., Irwin, J., McCaughrean, M. J., Baraffe, I., and Bertin,

E. (2008). Brown dwarfs and very low mass stars in the Hyades cluster: a dynamically evolved mass function. *A&A*, 481:661–672.

Chabrier, G., Baraffe, I., Allard, F., and Hauschildt, P. (2000). Evolutionary Models for Very Low-Mass Stars and Brown Dwarfs with Dusty Atmospheres. *ApJ*, 542:464–472.

Cropper, M. and Katz, D. (2011). The Gaia spectroscopic instrument (RVS): a technical challenge. In *EAS Publications Series*, volume 45 of *EAS Publications Series*, pages 181–188.

Cushing, M. C., Rayner, J. T., and Vacca, W. D. (2005). An Infrared Spectroscopic Sequence of M, L, and T Dwarfs. *ApJ*, 623:1115–1140.

Dawson, P., Scholz, A., and Ray, T. (2011). New brown dwarfs in the south part of the Upper Scorpius Association. *MNRAS (in press)*.

Kearney, K. J. and Ninkov, Z. (1998). Characterization of a digital micromirror device for use as an optical mask in imaging and spectroscopy. *Proceedings of SPIE*, 3292:81 – 92.

Kelsall, T., Weiland, J. L., Franz, B. A., Reach, W. T., Arendt, R. G., Dwek, E., Freudenreich, H. T., Hauser, M. G., Moseley, S. H., Odegard, N. P., Silverberg, R. F., and Wright, E. L. (1998). The COBE Diffuse Infrared Background Experiment Search for the Cosmic Infrared Background. II. Model of the Interplanetary Dust Cloud. *ApJ*, 508:44–73.

Kerber, F., Nave, G., and Sansonetti, C. J. (2008). The Spectrum of Th-Ar Hollow Cathode Lamps in the 691-5804 nm region: Establishing Wavelength Standards for the Calibration of Infrared Spectrographs. *ApJS*, 178:374–381.

Kiss, C., Pál, A., Müller, T. G., and Ábrahám, P. (2008). The impact of main belt asteroids on infrared-submillimetre photometry and source counts. *A&A*, 478:605–613.

Liermann, A., Hamann, W.-R., and Oskinova, L. M. (2009). The Quintuplet cluster. I. A K-band spectral catalog of stellar sources. *A&A*, 494:1137–1166.

Lindegren, L. (2010). High-accuracy positioning: astrometry. *ISSI Scientific Reports Series*, 9:279–291.

Lodieu, N., Hambly, N. C., and Jameson, R. F. (2006). New members in the Upper Scorpius association from the UKIRT Infrared Deep Sky Survey Early Data Release. *MNRAS*, 373:95–104.

Meyer, R. D., Kearney, K. J., Ninkov, Z., Cotton, C. T., Hammond, P., and Statt, B. D. (2004). Ritmos: a micromirror-based multi-object spectrometer. *Proceedings of SPIE*, 5492:200 – 219.

Miklós, M. (1998). Csillagászat. Akadémia Kiadó, Budapest.

Moraux, E., Bouvier, J., Stauffer, J. R., and Cuillandre, J.-C. (2003). Brown dwarfs in the Pleiades cluster: Clues to the substellar mass function. *A&A*, 400:891–902.

Nishiyama, S., Tamura, M., Hatano, H., Kato, D., Tanabé, T., Sugitani, K., and Nagata, T. (2009). Interstellar Extinction Law Toward the Galactic Center III. *ApJ*, 696:1407–1417.

Perryman, M. A. C., Cropper, M., Ramsay, G., Favata, F., Peacock, A., Rando, N., and Reynolds, A. (2001). High-speed energy-resolved STJ photometry of the eclipsing binary UZ For. *MNRAS*, 324:899–909.

Slesnick, C. L., Carpenter, J. M., and Hillenbrand, L. A. (2006). A Large-Area Search for Low-Mass Objects in Upper Scorpius. I. The Photometric Campaign and New Brown Dwarfs. *AJ*, 131:3016–3027.

Urgoiti, E., Ramirez, A., and Coste, P. (2005). GAIA M2M pointing mechanism. http://adsabs.harvard.edu/abs/2005ESASP.591...47U.

Wallace, L. and Hinkle, K. (1997). Medium-Resolution Spectra of Normal Stars in the K Band. *ApJS*, 111:445–+.

Wertz, J. R. Larson, W. J. (2008). *Space Mission Analysis and Design*. Springer.

Whitworth, A., Bate, M. R., Nordlund, Å., Reipurth, B., and Zinnecker, H. (2007). The Formation of Brown Dwarfs: Theory. *Protostars and Planets V*, pages 459–476.

Wilkinson, M. I., Vallenari, A., Turon, C., Munari, U., Katz, D., Bono, G., Cropper, M., Helmi, A., Robichon, N., Thévenin, F., Vidrih, S., Zwitter, T., Arenou, F., Baylac, M.-O., Bertelli, G., Bijaoui, A., Boschi, F., Castelli, F., Crifo, F., David, M., Gomboc, A., Gómez, A., Haywood, M., Jauregi, U., de Laverny, P., Lebreton, Y., Marrese, P., Marsh, T., Mignot, S., Morin, D., Pasetto, S., Perryman, M., Prša, A., Recio-Blanco, A., Royer, F., Sellier, A., Siviero, A., Sordo, R., Soubiran, C., Tomasella, L., and Viala, Y. (2005). Spectroscopic survey of the Galaxy with Gaia- II. The expected science yield from the Radial Velocity Spectrometer. *MNRAS*, 359:1306–1335.

Zacharias, N. and Dorland, B. (2006a). The Concept of a Stare-Mode Astrometric Space Mission. *PASP*, 118:1419–1427.

Zacharias, N. and Dorland, B. (2006b). The Concept of a Stare-Mode Astrometric Space Mission. *PASP*, 118:1419–1427.

Zamkotsian, F., Lanzoni, P., Grassi, E., Barette, R., Fabron, C., Tangen, K., Valenziano, L., Marchand, L., and Duvet, L. (2011). Successful evaluation for space applications of the 2048×1080 DMD. In *Society of Photo-Optical Instrumentation Engineers (SPIE) Conference Series*, volume 7932 of *Society of Photo-Optical Instrumentation Engineers (SPIE) Conference Series*.